

Björn Pfeiffelmann¹
Michael Diederich¹
Fethi Gül¹
Ali Cemal Benim^{1,*}
Markus Heese²
Andreas Hamberger²


Computational and Experimental Investigation of an Industrial Biomass Furnace

An industrial biomass boiler of 200 kW thermal power is analyzed by computational and experimental methods. Gas composition and temperature within the furnace and in the downstream heat exchanger are measured. Combustion, flow and heat transfer processes within the furnace, exhaust tract as well as the forced convection on the water side of the heat exchanger are computationally investigated by the finite volume method-based computational fluid dynamics procedures. The predictions are compared with the experiments. A satisfactory overall agreement between the predicted and measured temperatures is observed with an average deviation about 5 %. For oxygen mole fractions a fair agreement is found that shows deviations within the range of 10–20 %. For carbon monoxide, calculations exhibit a stronger underprediction.

Keywords: Biomass furnace, Combustion, Computational fluid dynamics, Waste wood

Received: November 29, 2019; *revised:* February 07, 2020; *accepted:* April 22, 2020

DOI: 10.1002/ceat.201900637

 This is an open access article under the terms of the Creative Commons Attribution-NonCommercial-NoDerivs License, which permits use and distribution in any medium, provided the original work is properly cited, the use is non-commercial and no modifications or adaptations are made.

1 Introduction

To generate heat and power [1, 2], combustion is being utilized as a major technology since many decades [3–6]. Parallel to efforts for exploiting renewable energies [7] as well as recovery techniques [8, 9], combustion continues to play an important role in renewable energies. This is due to the biomass [10–13], the utilization of which is the main focus of the present contribution. Biomass is a broadly available renewable fuel with advantages compared to fossil fuels. It is carbon-neutral and has low sulfur and ash contents compared to coal. Especially in decentralized utilization, it has the advantage of higher flexibility compared to other renewable energy sources.

The present paper presents the first step of a research project, which addresses biomass combustion as well as cogeneration [14]. The purpose is the development of a waste wood burning boiler with simultaneous generation of electric power. As cogeneration via organic Rankine cycle is also an option, thermoelectric generators [9, 15] are aimed to be used, due to their advantage of being maintenance-free and scalable for low power. This is to be achieved by implementing the necessary design modifications on an existing industrial boiler to lead to a prototype of a pilot cogenerating unit.

To assist and guide the intended development, a computational model of the boiler is developed in the present investigation. An existing waste wood boiler, which has been chosen as the starting point for the intended development, is analyzed computationally. Measurements are also performed for assessing the accuracy of the computational procedures.

In the present configuration, wood chips are fed by a screw at the bottom of the furnace. Thus, the combustion mode is

similar to grate firing. Many researchers applied computational fluid dynamics (CFD) procedures to simulate biomass combustion in grate furnaces. In one of the early studies, Scharler et al. [16] analyzed biomass grate firing using a global reaction scheme with the eddy dissipation model (EDM) [17], and proposed a modification of a model constant. Klason and Bai [18] presented a similar analysis applied to a small-scale furnace and also calculated NO formation. Klason et al. [19] investigated radiation modeling in biomass furnaces and found that a spectral line weighted-sum-of-grey-gases [20] model delivered the most accurate results, whereas the P1 model [21] also provides useful results for the furnace temperature distribution.

The effect of fly ash on radiation properties was investigated by Bahador and Sunden [22]. Comprehensive reviews of numerical simulation of biomass grate firing were provided by Yin et al. [23] and Chaney et al. [24]. In the more recent work of Kurz et al. [25], the focus was two-phase modeling for the interaction between the bed and freeboard. For a laboratory grate biomass furnace, Buchmayr et al. [26] used the steady flamelet model (SFM) and the eddy dissipation concept EDC

¹Björn Pfeiffelmann, Michael Diederich, Dr.-Ing. Fethi Gül, Prof. Dr.-Ing. habil. Ali Cemal Benim
alicemal@prof-benim.com

Düsseldorf University of Applied Sciences, Center of Flow Simulation, Department of Mechanical and Process Engineering, Münsterstrasse 156, 40476 Düsseldorf, Germany.

²Markus Heese, Andreas Hamberger
Endress Holzfeuerungsanlagen, Industriestrasse 18, 91593 Burgberheim, Germany.

[27] and concluded that SFM delivers a useful and comparably inexpensive alternative for a detailed combustion modeling. In a rather recent study by Farokhi et al. [28] on a laboratory furnace, in addition to SFM and EDC, the unsteady flamelet model was also applied. Farokhi et al. [28] concluded that EDC is more reliable for the prediction of the slow-chemistry species, where all three models were similarly capable of predicting the temperature and the major species profiles.

In the present work, an industrial wood chip burning boiler is numerically and experimentally investigated. The applied mathematical and numerical results are assessed by comparisons with the measurements. In comparison to the majority of the previous work, where rather small-scale laboratory furnaces were analyzed, an industrial furnace with a nominal thermal power of 200 kW is investigated. Furthermore, the water side of the boiler is also simulated, which served to describe the boundary conditions for the simulation of the furnace and the exhaust gas tract. A challenge in modeling boilers of this type is the close coupling of the furnace and the heat exchanger (gas to water), which are governed by completely different transport phenomena. An important goal of the present study is to develop a validated computational procedure for modeling such a complex system with a coupled treatment of the gas and water domains. The developed procedure will be used to guide the further development of the furnace for the intended integration of the thermoelectric generators for the purpose of cogeneration.

2 Investigated Boiler

The investigated boiler is an industrial under-feed wood chips fueled boiler with a nominal thermal power of 200 kW. The waste wood chips are transported by a screw through a channel at the bottom of the furnace. The ash is pushed out of the furnace by the action of the fuel feeding screw and additional ash screw. The net calorific value of the fuel is 17 MJ kg⁻¹. The fuel composition is presented in Tab. 1.

The water domain of the boiler encloses the furnace. The water temperature is kept below the atmospheric boiling point. A sketch of the boiler is provided in Fig. 1, where the measuring points and planes are also indicated.

The primary air is injected into the fuel bed, with a resulting equivalence ratio ϕ of 0.95. The pyrolysis products and the products of partial combustion enter into the secondary combustion zone as a gaseous mixture, where they are mixed with the secondary air to lead to complete combustion. The secondary air is injected as jets through a number of nozzles. The overall equivalence ratio is 0.49.

Combustion products thermally interact with the cold surface of the

Table 1. Fuel properties.

Parameter	Mass fraction
<i>Proximate analysis</i>	
Ash	0.017
Fixed carbon	0.181
Moisture	0.061
Volatile matter	0.741
<i>Ultimate analysis (dry, ash-free)</i>	
C	48.0
H	6.1
N	4.7
O	41.2

boiler wall by convection and radiation, and cool down. To extract the remaining energy, the gas is conducted through two passes of convective heat exchangers consisting of tube rows. Tubes in the second pass are equipped with twisted tapes inserts. They enhance the convective heat transfer and provide means to clean the surfaces.

3 Experimental

The fuel mass flow rate is determined by gravimetry. Flow rates of primary and secondary air and exhaust gas are assessed by measuring the velocity profiles by pitot tubes. Temperatures in the furnace and in the convective heat exchanger are measured by thermocouples. In the furnace, the temperature difference between the gas and boiler walls is large. To minimize radiation effects on temperature measurement, a cooled suction pyrometer is used. Subsequently, the gas is sucked by a flue gas

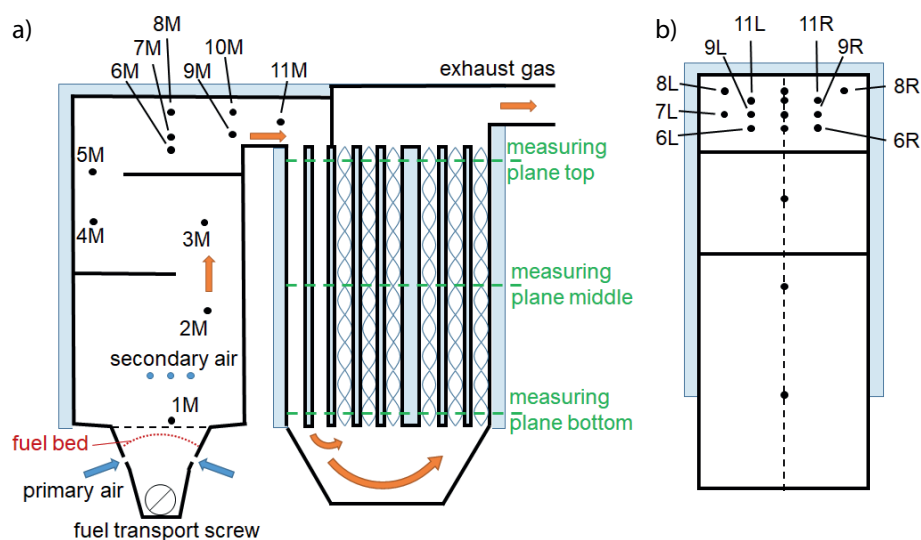


Figure 1. Sketch of the boiler with measuring points and planes: (a) side view, (b) front view.

analyzer to detect oxygen and carbon monoxide concentrations. In the convective heat exchanger, blank thermocouples are used. The temperatures on the external boiler walls are also obtained by thermocouples.

In Fig. 1a, the measuring points are indicated, which are all placed along the middle plane through the furnace, where the symbol M stays for “middle”. In the highest pass of the furnace, there are measuring points that are placed left and right of the middle plane. They are indicated in Fig. 1b, with the symbols L and R staying for “left” and “right”, respectively (the points are not in the same plane). In addition, gas temperatures are determined at several points along horizontal planes in the convective heat exchanger that are indicated as measuring planes “top”, “middle”, and “bottom” in Fig. 1a.

Due to the intermittent fuel feed with a cycle rate of about 1 min, the process has a periodic unsteadiness apart from turbulence or possible variations due to fuel properties. Thus, the measurements have been performed for a time span of 30 min with a sample rate of 1 s, logged by a data logger, and the time-averaged values are taken as the measured value to compare with the steady-state simulation results.

4 Modeling

4.1 Outline of the Mathematical and Numerical Modeling

For the computational modeling, the finite volume method-based CFD code ANSYS Fluent 2019 R3 [29] is used. The governing equations are solved in 3D domains in steady state. While the water is incompressible, the gas mixture density is calculated from the ideal gas thermal equation-of-state. Buoyancy effects are neglected. Constant values are assigned to molecular transport and the specific heat capacity of water that correspond to a representative mean temperature. Temperature dependences of the specific heat capacities of gaseous components are considered via fourth-order polynomials. A coupled solver is used. For discretizing the convective terms, a second-order accurate upwind scheme is applied [30]. Turbulence is modeled by the Standard k - ϵ model [31]. Enhanced wall functions [32] are selected for the near-wall flow.

4.2 Definition of Subdomains

A challenge has been the coupling between the gas and the water domains. Measurements have indicated that great amounts of heat are transferred to water through the upper portions of the furnace walls. A fully coupled treatment of the gas (furnace) and water domains would theoretically be possible, but rather inconvenient due to the complex geometries involved and different flow physics. Thus, the water and gas domains are treated in separate calculation domains that are coupled via thermal boundary conditions. The gas domain is also split into two, where the furnace with combustion and the exhaust tract without combustion are treated separately.

At inlets, homogeneous profiles are applied for velocity, temperature, and composition. Inlet values of turbulence quantities

are based on an assumed turbulence intensity of 5% and the hydraulic diameter. An exception is the inlet of the second gas domain (exhaust track), where the outlet distributions of the first gas domain (furnace) are directly applied as inlet boundary conditions. Static pressure is prescribed at outlets along with the zero normal gradient conditions for other variables. For radiation, inlet and outlet surfaces are assumed to be black. On solid walls, no-slip conditions hold for the momentum equations. The thermal boundary conditions will be described in more detail below.

In Fig. 1b, one can see that the geometry is symmetric about the middle plane as indicated by the dashed line. However, the fuel is driven from left to right, disturbing the symmetry. Nevertheless, in the computational model, such an asymmetry is not considered since constant inlet profiles were prescribed. Thus, in the computations, half domains are considered utilizing the symmetry.

4.3 Modeling the Water Domain

The main purpose of the water domain calculation has been to determine convective heat transfer coefficients to be used as thermal boundary conditions for the gas domain. For “cold boundaries” of the water domain that interact with external boiler walls, the measured wall temperatures are employed as boundary conditions. Within the domain, the water temperature varies in a rather small range of about 10 K. Consequently, the change of the material properties is also not significant. Under these conditions, the convective heat transfer coefficients are not significantly dependent on the wall temperature [33]. This leads to a weak coupling between domains, without necessarily requiring a large number of iterations.

4.4 Modeling the Exhaust Track

The non-reacting flow of the gas mixture with the inlet conditions borrowed from the outlet of the furnace is modeled through a number of tubes arranged in two passes (Fig. 1). The inlet boundary of this domain is placed about the horizontal plane labeled as “measuring plane top” in Fig. 1a. The thermal boundary conditions on the walls, which separate gas from water, are formulated using the convective heat transfer coefficients resulting from the water domain analysis. The heat conduction through the solid walls that separate the gas from the water is also considered in formulating the boundary condition assuming a 1D heat conduction; the same holds for the furnace domain, too. Walls of the twisted tape inserts are assumed to be adiabatic. Radiative heat transfer is also considered in this domain.

4.5 Modeling the Furnace

Modeling of this sub-domain is most demanding, as far as the complexity of the mathematical formulation is concerned. The modeling of the processes in the fuel bed is a great challenge for its own. In the present approach, the inlet boundary is

placed slightly above the fuel bed, as indicated by the horizontal dashed line in Fig. 1a, just below the measuring point 1M. It is assumed that the gaseous products of the pyrolysis and partial combustion can be represented by an adequate composition of gaseous species at this inlet plane. Based on the given fuel composition, trying to capture all hydrogen in a hydrocarbon that gives a similar C/H ratio in the volatile matter, the latter is assumed to be made up of C_2H_6 . The remaining fixed carbon is assumed to have reacted to CO in bed vicinity. This implies an increased temperature due to the assumed CO formation. This is compared with the measured temperature above the bed (1M), and it was observed that the latter was higher.

As already mentioned, the primary air injection leads to an excess air ($\varphi = 0.95$) in the bed, which enhances the combustion and leads to the observed high temperature. The measured high temperature is assumed to be attained by a further reaction of the assumed gaseous mixture upstream the measuring point 1M. Calculation of these reactions were performed using the detailed reaction mechanism GRI-Mech 3.0 [34] with the chemical kinetics solver Cantera [35], in a 1D laminar pre-mixed flame configuration. The state corresponding to the measured inlet temperature at 1M is then prescribed as the inlet temperature and the inlet gas composition, summarized in Tab. 2.

Table 2. Inlet gas composition (mole fraction).

	C_2H_6	CO	O_2	CO_2	H_2O	N_2
X_i [%]	0.2	7.4	6.9	6.7	11.3	67.5

Note that this analysis is based on a temperature measured at a single point and thus afflicted with a large uncertainty when used to represent the state for the whole inlet surface. However, with the limited accessibility, it was not possible to take measurements at more than one point close to the freeboard.

The P1 method [21, 36] is applied for calculating the radiative heat transfer. The gas absorption coefficient is calculated by the weighted-sum-of-grey-gases method [37], using a domain-based mean beam length [36]. The effect of fly ash on the radiation properties of the gas mixture is neglected. Although no measurements on the fly ash could be performed, an estimation based on ref. [22, 38] indicated that its effect on the mixture absorption coefficient should be less than 6%, which can be seen as a justification of this omission. The wall emissivities are assumed to be 0.8 [39].

4.6 Combustion Modeling

For combustion of the gaseous mixture, two reaction mechanisms are considered. The first one is a two-step global reaction mechanism consisting of five reaction species, where C_2H_6 reacts to CO and H_2O in the first reaction and CO to CO_2 in the second reaction. For the kinetic rate constants, the values suggested by Westbrook and Dryer (WD) [40] are employed. For obtaining a more accurate description, the semi-detailed

DRM22 mechanism is used, which comprises 22 species. This was developed by Kazakov and Frenklach [41] truncating the full Gri-Mech 1.2.

For modeling turbulence-chemistry interaction, two approaches are used: the eddy dissipation model (EDM) [20] and the eddy dissipation concept (EDC) [31]. In using EDM, the chemistry effects are taken into account by calculating the conversion rates according to chemical kinetics by neglecting turbulence fluctuations, comparing them with those of EDM and taking the smaller one as the effective conversion rate. EDM is applied only with the WD mechanism, EDC with both mechanisms.

4.7 Computational Grids

The domains have complex geometries, and grid generation in all three domains is challenging. Unstructured grids are used. Fig. 2 displays the variation of the gas temperature and O_2 mole fraction calculated (EDM WD) in the furnace at three measuring points (Fig. 1) for three grids. One can see that a grid-independent solution can be assumed for the finest grid with 5×10^6 cells. Grid independence studies have been performed for the other domains, too. The resulting grids for the exhaust track and water domains consisted of about 8×10^6 and 6×10^6 cells, respectively. In all domains, the resulting maximum local y^+ values did not exceed 60.

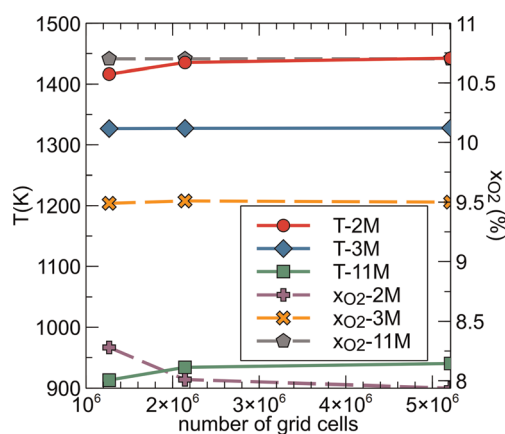


Figure 2. Variation of calculated temperatures and O_2 mole fractions with grid resolution.

5 Results

5.1 Furnace Domain

5.1.1 Field Distributions

Distributions of velocity magnitude, temperature, and O_2 mass fraction as predicted by EDM WD in the furnace domain are displayed in Fig. 3. A secondary air jet in the plane can be recognized.

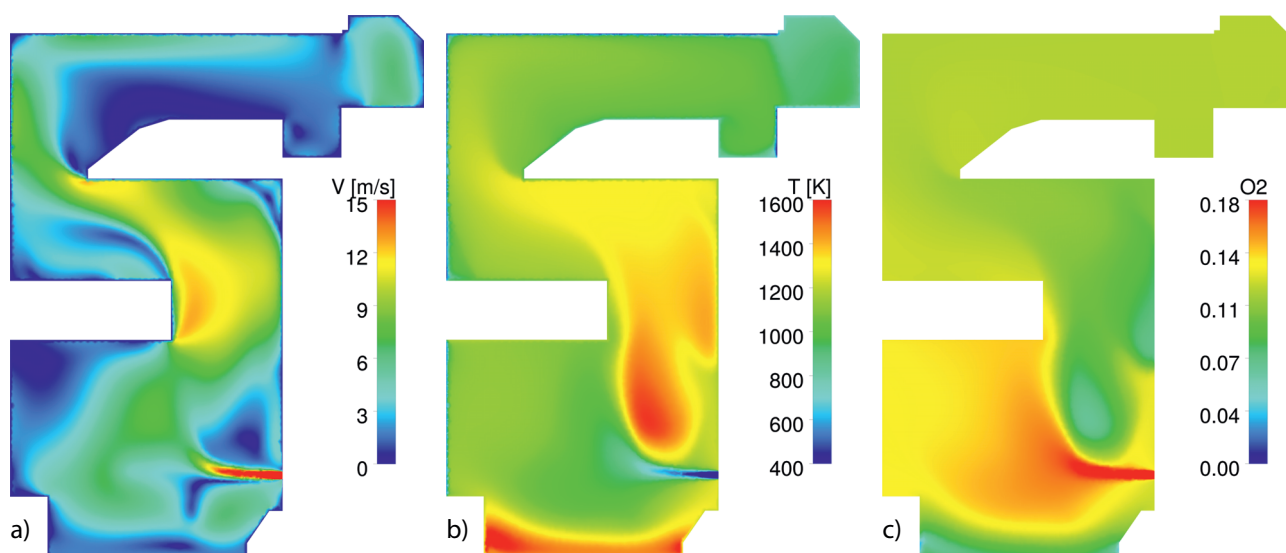


Figure 3. Predicted distributions in the furnace in the symmetry plane: (a) velocity magnitude, (b) temperature, (c) O₂ mass fraction.

The high jet velocity and flow acceleration at the exit of the primary combustion section as well as low velocity recirculation regions can be observed in Fig. 3a. The deflections along the gas path create local regions of increased velocity. This phenomenon at the upmost deflection plays an important role for the convective heat transfer from the furnace. The high velocity values along the cooled upper wall (Fig. 3a) cause increased values of the local convective heat flux. As discussed above, high temperatures at the domain inlet can be recognized. A local temperature maximum occurs by the burnout achieved by the action of the secondary air jets (Fig. 3b). A local depletion of O₂ in the burnout zone can be observed in Fig. 3c.

5.1.2 Comparison of Predictions with Measurements

Predicted temperatures by the three combustion modeling approaches are compared with the measurements at the measuring points in the furnace (Fig. 1) in Fig. 4. Note that the “left” (L) and “right” (R) measuring points (Fig. 1b) are displayed in the same figure (Fig. 4b). In most cases, they are nearly identical and cannot be recognized as different values. For the points 6L, 6R (6LR, Fig. 4b) a slight difference is observed. This confirms the assumption of patterns in the furnace to be nearly symmetric.

For all models, a good qualitative overall agreement between the predicted and measured temperatures is found (Fig. 4). From the deviations between the measurements and predictions, implications for the qualitative performance of the models can be drawn. In the experiments, the secondary combustion zone seems to be located in the vicinity of the point 3M, as indicated by the measured local maximum temperature at this point. All models predict a faster reaction progress in the secondary combustion zone as implied by the higher temperatures predicted at more upstream positions (2M), which is especially pronounced for EDM (Fig. 4a).

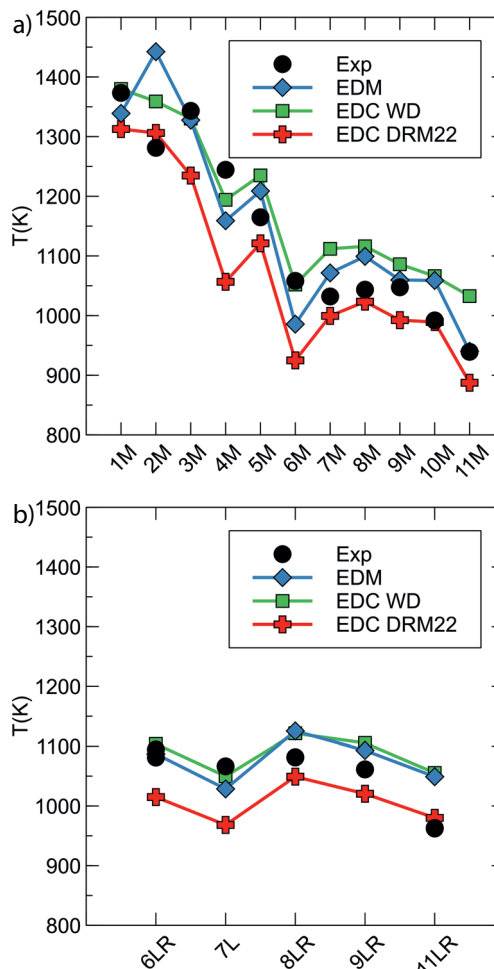


Figure 4. Temperatures at measuring points in the furnace: (a) in middle plane, (b) on left and right.

For the upmost channel of the gas tract, a comparison of the measured temperatures in the middle of the channel (6M, 7M, 8M, Fig. 4a) with the corresponding temperatures at the points sideward in the channel (6LR, 7L, 8LR, Fig. 4b) demonstrates that the temperatures at the sideward points are higher than those at the middle. As similar trend can be observed comparing the measured temperatures at 9M and 11M (Fig. 4a) with 9LR and 11LR (Fig. 4b), respectively. This is caused by the secondary flows generated by the flow deflection at the beginning of the channel, which convey cold fluid from the cooled upper wall to the channel center. This phenomenon is also predicted by the computational models, which show a good qualitative agreement with the measurements (Fig. 4). Also quantitatively, the models exhibit a satisfactory overall performance. Mean percentage deviations of the predicted temperatures from the measured ones are calculated for all three models. Deviations are arithmetically averaged over the points indicated in Fig. 4. These mean deviations turn out to be 4.5 % for EDM WD, 5.3 % for EDC WD, 5.3 % for EDC DRM22. The temperature at the exit of the furnace (points 11M, 11LR, Fig. 4) is predicted closely by EDC DRM22 and similarly good by EDM WD.

Predicted O_2 mole fractions by the three combustion modeling approaches are compared with the measurements at the measuring points in the furnace in Fig. 5. One can see that the predictions show a similar qualitative trend to each other. However, the position of the experimentally observed second peak in the vertical distribution is shifted in the predictions (Fig. 5a). The observed local minima in the oxygen mole fractions (Fig. 5a) relate with the above discussion of the temperature profile (Fig. 4a) with respect to the position of the secondary combustion zone. Here, it is even more clearly seen that the models predict the combustion zone to be located around point 2M. The measurements demonstrate that it is at a further downstream position, around point 3M, which means an over-prediction of the reaction progress in this zone.

Quantitatively, the EDM WD and EDC DRM22 predictions agree very well with each other but overpredict the experimental values beyond the point 3M. The EDC WD prediction differs quantitatively from the other predictions and agrees better with the experiments. The mean percentage deviations of the predictions from the experiments turn out to be larger for the O_2 mole fractions than it has been for the temperatures. The mean percentage deviations for the O_2 mole fractions are calculated to be 18.0 %, 11.8 %, and 17.7 % for the models EDM WD, EDC WD, and EDC DRM22, respectively.

The predicted CO mole fractions by the three combustion modeling approaches are compared with the measurements at measuring points along the furnace height in Fig. 6. It is observed that all models underpredict the measured values. EDC DRM22 results are comparably closer to experiments, while EDM predicts the lowest values.

5.2 Exhaust Track and Water Domains

5.2.1 Field Distributions

The predicted temperature distributions in the convective heat exchanger tubes are displayed in Fig. 7. For these calculations,

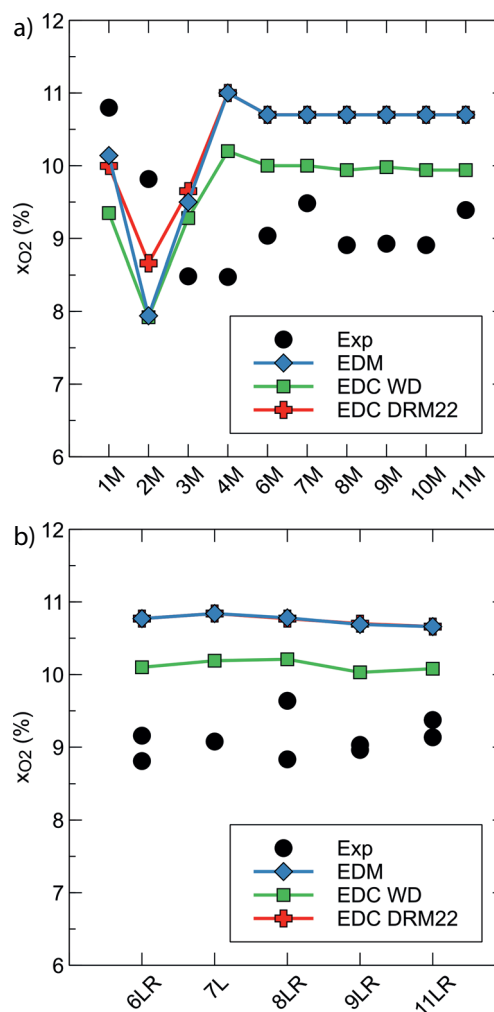


Figure 5. O_2 mole fractions at measuring points in the furnace: (a) in middle plane, (b) on left and right.

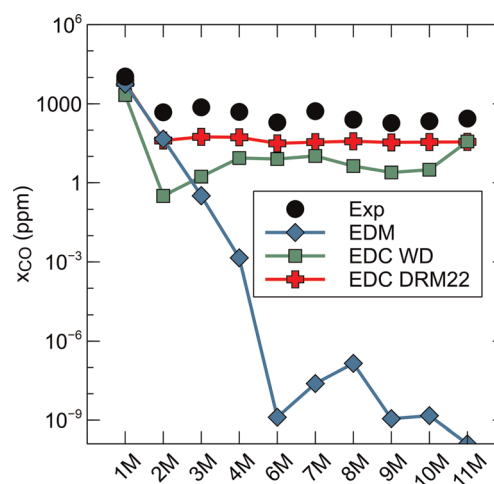


Figure 6. CO mole fractions at measuring points along the furnace height.

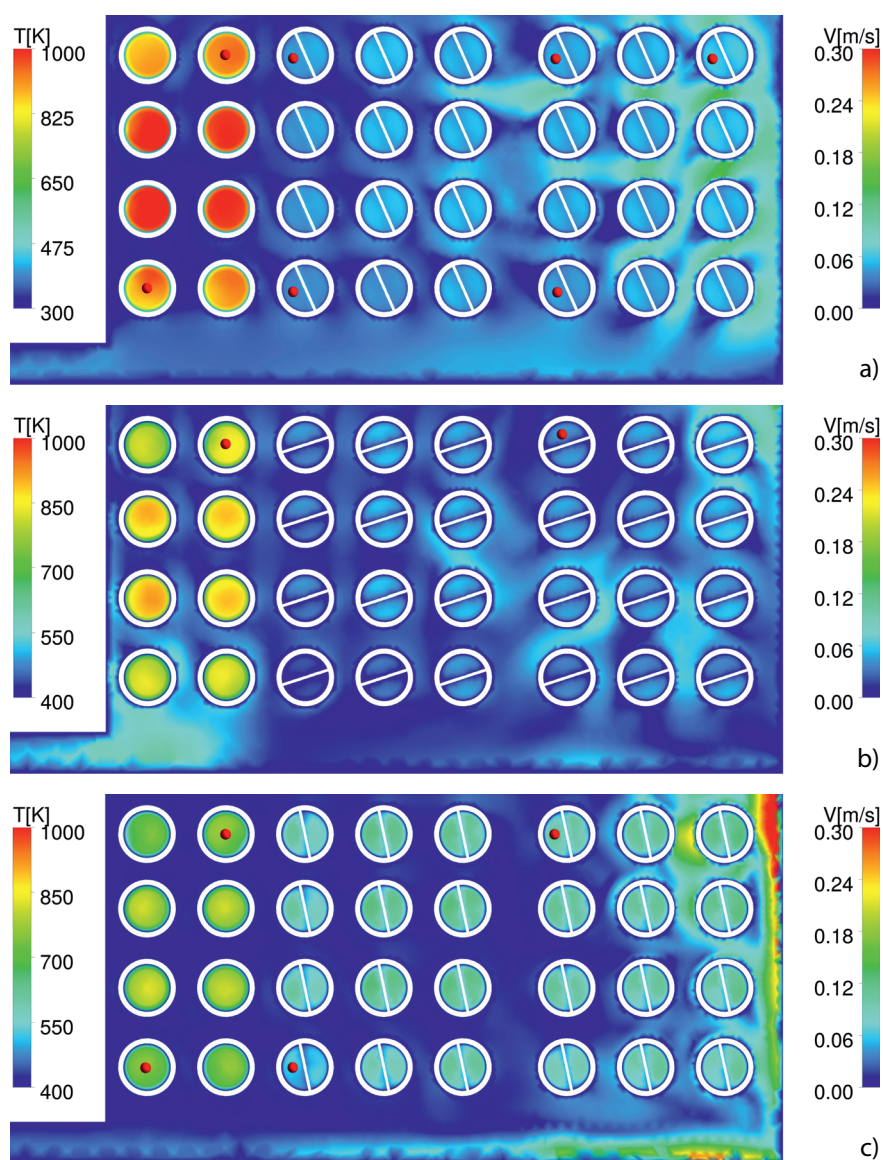


Figure 7. Predicted gas temperature and water velocity in horizontal measuring planes: (a) top, (b) middle, (c) bottom.

the inlet boundary conditions for the exhaust track were based on the EDC DRM22 calculation of the furnace. The temperatures (T) are displayed in the three measuring planes “top”, “middle” and “bottom” indicated in Fig. 1a. The circular cross sections of the tubes as well as the rectangular cross sections of the twisted tapes fitted in the tubes of the second pass can be recognized. The red points indicate the positions of the temperature measurement points. The points are not labeled for not disturbing the appearance. In addition to the gas temperature field in the tubes, the velocity field of the water outside the tubes is also displayed in the figure, plotting the magnitude of the water velocity (V) in the cross sections. The nonhomogeneous lateral distribution of the gas temperature in the upmost furnace channel was discussed above, where lower gas temperatures in the middle of the channel were measured and pre-

dicted compared to temperature values sideward. As consequence, a corresponding inhomogeneity for the gas temperature is observed in the inlet section of the first pass tubes of the heat exchanger (Fig. 7a).

One can see how the gas temperature decreases in the downward direction from top to bottom and upward from bottom to top direction in the first and second pass of the heat exchanger, respectively. A quite inhomogeneous distribution of the water velocity can also be observed (Fig. 7).

5.2.2 Comparison of Predictions with Measurements

In Fig. 8, the predicted temperatures are compared with the measured ones for the measuring points (red points in Fig. 7). The predicted exhaust gas temperatures agree qualitatively and quantitatively quite well with the measured values (Fig. 8). One can also observe that the percentage deviation between the measurements and predictions is smaller for the points in the first pass compared to those in the second pass. The geometry of the tubes in the second pass was complicated due to the twisted tapes and some simplifications and idealizations had to be done in their modeling. This is assumed to be the cause of the comparably less accurate prediction for the second pass. As an overall assessment, it is observed that the average deviation of the predicted values from the measurements is 5.0 %, which can be considered to be quite satisfactory.

6 Conclusions

An industrial waste wood burning boiler with a nominal thermal power of 200 kW is analyzed by means of computational and experimental methods. Combustion, flow, and heat transfer processes within the furnace, exhaust tract as well as the forced convection on the water side of the heat exchanger are evaluated. The main findings are summarized below:

- A satisfactory overall agreement between the predicted and measured temperatures is observed with an average deviation of about 5 %.
- For oxygen mole fractions a less accurate but a still fair agreement is obtained that shows deviations within the range of 10–20 %. For carbon monoxide, the calculations exhibit a larger underprediction of the measured values.

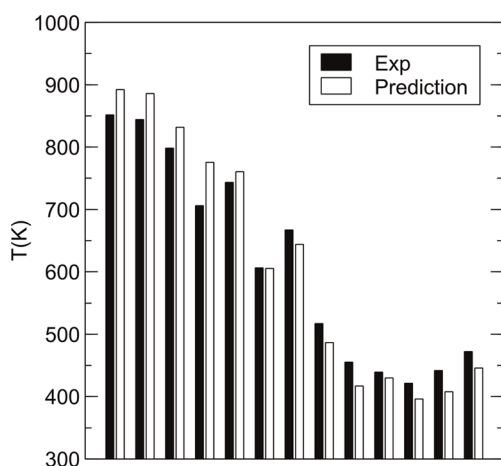


Figure 8. Gas temperatures at measuring points along the exhaust track.

- Although combustion models with different degrees of sophistication are applied, the predictions of temperature and concentrations are observed not to depend strongly on the combustion model. The reason is expected to be due to the substantial progress of combustion in the close vicinity of the fuel bed, which remains outside of the present computational domain, but is considered via inlet boundary conditions that are derived under some assumptions and prescribed to be the same for all models.
- A more accurate modeling of the combustion in the fuel bed and its interaction with the gas flow over the freeboard is aimed for the future.

Acknowledgment

The results presented in this paper were obtained from the project “Biomassseg”. This project was funded by the funding section “Biomass energy use” of the German Ministry of Economic Affairs and Energy in the framework of the 7. Energy Research Program. Open access funding enabled and organized by Projekt DEAL.

The authors have declared no conflict of interest.

Symbols used

k	$[\text{m}^2\text{s}^{-2}]$	turbulence kinetic energy
T	$[\text{K}]$	temperature
V	$[\text{m s}^{-1}]$	velocity magnitude
X_i	$[-]$	mole fraction of species i
y^+	$[-]$	dimensionless wall distance

Greek letter

ε	$[\text{m}^2\text{s}^{-3}]$	dissipation rate of k
φ	$[-]$	equivalence ratio

Abbreviations

CFD	computational fluid dynamics
EDC	eddy dissipation concept
EDM	eddy dissipation model
L	left point
M	middle point
R	right point
SFM	steady flamelet model
WD	Westbrook and Dryer

References

- [1] P. Breeze, *Power Generation Technologies*, 2nd ed., Newnes, Oxford **2014**.
- [2] A. C. Benim, M. Geiger, S. Doehler, M. Schoenenberger, H. Roemer, *Modelling the flow in the exhaust hood of steam turbines under consideration of turbine-exhaust hood interaction*, VDI Berichte, Vol. 1185, VDI Verlag, Düsseldorf **1995**, 343–357.
- [3] A. C. Benim, B. Epple, B. Krohmer, *Progr. Comput. Fluid Dyn.* **2005**, 5 (6), 345–361. DOI: <https://doi.org/10.1504/PCFD.2005.007067>
- [4] J. P. Kim, U. Schnell, G. Scheffknecht, A. C. Benim, *Prog. Comput. Fluid Dyn.* **2007**, 7 (6), 337–346. DOI: <https://doi.org/10.1504/PCFD.2007.014683>
- [5] A. C. Benim, M. P. Escudier, A. Nahavandi, A. K. Nickson, K. J. Syed, F. Joos, *Int. J. Numer. Methods Heat Fluid Flow* **2010**, 20 (3), 348–370. DOI: <https://doi.org/10.1108/09615531011024084>
- [6] A. C. Benim, S. Iqbal, W. Meier, F. Joos, A. Wiedermann, *Appl. Therm. Eng.* **2017**, 110, 202–212. DOI: <https://doi.org/10.1016/j.applthermaleng.2016.08.143>
- [7] R. Ehrlich, *Renewable Energy*, CRC Press, Boca Raton, FL **2013**.
- [8] *Energy Recovery* (Eds: E. DuBois, A. Mercier), Nova Science Publishers, New York **2009**.
- [9] D. G. Ebling, A. Krumm, B. Pfeiffelmann, J. Gottschald, J. Bruchmann, A. C. Benim, M. Adam, R. Labs, R. R. Herbertz, A. Stunz, *J. Electron. Mater.* **2016**, 45 (7), 3433–3439. DOI: <https://doi.org/10.1007/s11664-016-4511-8>
- [10] *Energy from Organic Materials (Biomass)* (Ed: M. Kaltschmitt), Springer, New York **2019**.
- [11] E. Acikkalp, T. Zeng, A. Ortwein, H. Burkhardt, W. Klenk, *Chem. Eng. Technol.* **2018**, 41 (11), 2141–2149. DOI: <https://doi.org/10.1002/ceat.210800041>
- [12] J. D. Smith, A. Alembath, H. Al-Rubaye, J. Yu, X. Gao, H. Golpour, *Chem. Eng. Technol.* **2019**, 42 (12), 2505–2519. DOI: <https://doi.org/10.1002/ceat.201900304>
- [13] X. Shi, J. Gao, X. Lan, *Chem. Eng. Technol.* **2019**, 42 (12), 2574–2579. DOI: <https://doi.org/10.1002/ceat.201900085>
- [14] *Micro Cogeneration* (Eds: M. Pehtnt, M. Cames, C. Fischer, B. Praetorius, L. Schneider, K. Schumacher, J.-P. Voß), Springer, Berlin **2006**.
- [15] *Thermoelectrics Handbook* (Ed: D. M. Rowe), CRC Press, Boca Raton, FL **2006**.

- [16] R. Scharler, T. Fleckl, I. Obernberger, *Prog. Comput. Fluid Dyn.* **2003**, 3 (2–4), 102–111. DOI: <https://doi.org/10.1504/PCFD.2003.003776>
- [17] B. F. Magnussen, B. H. Hjertager, in *Proc. of the 16th Symp. (Int.) on Combustion*, The Combustion Institute, Pittsburgh, **1976**, 719–729.
- [18] T. Klason, X. S. Bai, *Fuel* **2007**, 86, 1465–1474. DOI: <https://doi.org/10.1016/j.fuel.2006.11.022>
- [19] T. Klason, X. S. Bai, M. Bahador, T. K. Nilsson, B. Sundén, *Fuel* **2008**, 87, 2141–2153. DOI: <https://doi.org/10.1016/j.fuel.2007.11.016>
- [20] M. K. Denison, B. W. Webb, *Trans. ASME J. Heat Transfer* **1995**, 117, 359–365. DOI: <https://doi.org/10.1115/1.2822652>
- [21] A. C. Benim, *Comput. Methods Appl. Mech. Eng.* **1988**, 67 (1), 1–14. DOI: [https://doi.org/10.1016/0045-7825\(88\)90065-5](https://doi.org/10.1016/0045-7825(88)90065-5)
- [22] M. Bahador, B. Sundén, *Int. J. Heat Mass Transfer* **2008**, 51, 2411–2417. DOI: <https://doi.org/10.1016/j.ijheatmasstransfer.2007.08.013>
- [23] C. Yin, L. A. Rosendahl, S. K. Kaer, *Prog. Energy Combust. Sci.* **2008**, 34, 725–254. DOI: <https://doi.org/10.1016/j.pecs.2008.05.002>
- [24] J. Chaney, H. Liu, J. Li, *Energy Convers. Manage.* **2012**, 63, 149–156. DOI: <https://doi.org/10.1016/j.enconman.2012.01.036>
- [25] D. Kurz, U. Schnell, G. Scheffknecht, *Prog. Comput. Fluid Dyn.* **2013**, 13 (5), 322–332. DOI: <https://doi.org/10.1504/PCFD.2013.055060>
- [26] M. Buchmeyer, J. Gruber, M. Hargassner, C. Hochenauer, *Energy Convers. Manage.* **2016**, 115, 32–42. DOI: <https://doi.org/10.1016/j.enconman.2016.02.038>
- [27] B. F. Magnussen, in *Proc. 19th AIAA Aerospace Science Meeting*, St. Louis, MO, January **1981**.
- [28] M. Farokhi, M. Birouk, F. Tabet, *Energy Convers. Manage.* **2017**, 143, 203–217. DOI: <https://doi.org/10.1016/j.enconman.2017.03.086>
- [29] ANSYS® *Fluent 2019 R3 Theory Guide*, ANSYS Inc., Canonsburg **2019**.
- [30] T. J. Barth, D. C. Jespersen, *AIAA-89-0366*, **1989**. DOI: <https://doi.org/10.2514/6.1989-366>
- [31] *Statistical Theory and Modeling for Turbulent Flows*, 2nd ed. (Eds: P. A. Durbin, B. A. Pettersson Reif), Wiley, Chichester **2011**.
- [32] B. A. Kader, *Int. J. Heat Mass Transfer* **1981**, 24 (9), 1541–1544. DOI: [https://doi.org/10.1016/0017-9310\(81\)90220-9](https://doi.org/10.1016/0017-9310(81)90220-9)
- [33] W. M. Kays, *Convective Heat and Mass Transfer*, McGraw-Hill, New York **1966**.
- [34] G. P. Smith, D. M. Golden, M. Frenklach, N. W. Moriarty, B. Eiteneer, M. Goldenberg, C. T. Bowman, R. K. Hanson, S. Song, W. C. Gardiner Jr., V. V. Lissianski, Z. Qin, <http://combustion.berkeley.edu/gri-mech/> (Accessed on May 01, 2019)
- [35] D. G. Goodwin, R. L. Speth, H. K. Moffat, B. W. Weber, *Cantera: An object-oriented software toolkit for chemical kinetics, thermodynamics and transport processes*, Version 2.4.0, **2018**. <https://www.cantera.org> (Accessed on May 01, 2019)
- [36] M. N. Özisik, *Radiative Transfer and Interactions with Conduction and Convection*, Wiley, New York **1973**.
- [37] T. F. Smith, Z. F. Shen, J. N. Friedman, *Trans. ASME J. Heat Transfer* **1982**, 104, 602–608. DOI: <https://doi.org/10.1115/1.3245174>
- [38] *VDI-Wärmeatlas* (Eds: VDI e.V.) Springer, Berlin **2013**. DOI: <https://doi.org/10.1007/978-3-642-19981-3>
- [39] J. P. Holman, *Heat Transfer*, 10th ed., McGraw-Hill Education, New York **2009**.
- [40] C. K. Westbrook, F. L. Dryer, *Combust. Sci. Technol.* **1981**, 27, 31–43. DOI: <https://doi.org/10.1080/00102208108946970>
- [41] A. Kazakov, M. Frenklach, <http://www.me.berkeley.edu/drm/> (Accessed on May 01, 2019)